The Role of Lower-Hybrid-Wave Collapse in the Auroral Ionosphere

P. W. Schuck* and G. I. Ganguli
Plasma Physics Division, Naval Research Laboratory, Code 6794, 4555 Overlook Avenue, SW, Washington, D.C. 20375-5000

P. M. Kintner
School of Electrical and Computer Engineering, Cornell University, Ithaca, New York 14853
(Received 23 January 2002; published 19 July 2002)

In regions where lower-hybrid solitary structures (LHSS) are observed, the character of auroral lower-hybrid turbulence (LHT) (0–20 kHz) is investigated using the amplitude probability distribution of the electric field. The observed probability distributions are accurately described by a Rayleigh distribution with two degrees of freedom. The statistics of the LHT exhibit no evidence of the global modulational instability or self-similar wave collapse. We conclude that nucleation and resonant scattering in preexisting density depletions are the processes responsible for LHSS in auroral LHT.

DOI: 10.1103/PhysRevLett.89.065002 PACS numbers: 52.35.Ra, 52.35.Fp, 52.35.Mw, 94.20.–y

Turbulence remains an important unsolved problem in plasma physics. Since Zakharov's seminal paper [1] on the self-modulation and self-similar collapse of strong Langmuir turbulence via the ponderomotive force, the theoretical community has expended great effort to describe the modulational instability and collapse of a variety of plasma modes. This Letter examines TOPAZ III sounding rocket data, a typical example of lower-hybrid tubulence (LHT) in the auroral ionosphere in which lower-hybrid solitary structures (LHSS) were observed [2,3]. Several authors have proposed that LHSS are the result of modulational instability and self-similar collapse [4–7]. We question the importance of these coherent processes in auroral turbulence where stochastic processes may dominate.

Lower hybrid turbulence, a fundamental process in many astrophysical phenomena, is a ubiquitous emission in the auroral ionosphere. LHT is broadband noise characterized by sharp lower cutoff at the local lower-hybrid resonance f_R determined by the cold electrostatic plasma dispersion relation $f_R = \omega_i/(2\pi\sqrt{1+\omega_e^2/\Omega_e^2})$ where $m_j (j = i, e)$ is the species mass, $\omega_j^2 = e^2 n_0/\epsilon_0 m_j$ is the species plasma frequency, n_0 is the plasma density, ϵ_0 is the permittivity of free space, e is the fundamental unit of charge, $\Omega_e = eB_0/m_e$ is the electron cyclotron frequency, and B_0 is the magnetic field strength. Frequently LHSS are observed in sounding rocket and satellite data below 2000 km [2,3,8–10]. These events consist of twofold to tenfold enhancements in electric field activity localized in stationary field-aligned cylindrical density depletions with depths of a few to tens of percent and widths of 20–100 m in diameter [8,10]. The correlation between large amplitude electric fields and density depletions motivated work [4] to explain these observations via a self-similar "soliton" collapse process which couples low-frequency density perturbations to high-frequency electric fluctuations through the *vector-type* ponderomotive potential

$$\delta n = i\frac{\epsilon_0\omega_e}{8\pi\Omega_e f_R}\frac{\hat{z}\cdot\tilde{\mathbf{E}}\times\tilde{\mathbf{E}}^*}{k_B(T_i+T_e)} \sim \mathrm{Im}(\tilde{E}_x\tilde{E}_y^*), \qquad (1)$$

where T_j is the species temperature and $\tilde{\mathbf{E}}$ is the complex slow envelope of the electric field: $\mathbf{E} = \mathrm{Re}[\tilde{\mathbf{E}}(t)\exp(i2\pi f_R t)]$. Statistical analysis of the LHSS observed by the Freja satellite has discounted collapse theory [4] because of large discrepancies between the theoretical predictions and the observed structure widths, density depths, electric field strengths, and pertinent time scales of LHSS [8,10]. However, the recent theoretical work of Robinson [7] rationalized these discrepancies using the modern theory of strong turbulence, a four phase *nucleation cycle* [5,7,11]: nucleation, collapse, arrest, and relaxation. According to this scenario [5,7], auroral LHT consists of wave packets of localized, coherent lower-hybrid (LH) states trapped in density depletions which are embedded in a background of incoherent turbulence.

During the nucleation phase, energy is transferred from the background turbulence to the nucleating LH states. If the potential of the wave packet exceeds the threshold

$$E_0\ell_\perp > \langle\Phi_c\rangle = \frac{15}{2^{1/4}}\frac{\Omega_e}{\omega_e}\sqrt{\frac{m_e}{m_i}\frac{T_i}{T_e}\left(1+\frac{T_i}{T_e}\right)}\frac{k_B T_e}{e}, \qquad (2)$$

self-similar collapse ensues with the ponderomotive potential producing a self-consistent density depletion or enhancement. Here E_0 is the electric field at the center of the wave packet, $\ell_\perp$ is the Gaussian half-width at half-maximum of the wave packet perpendicular to the magnetic field, and $\langle\Phi_c\rangle$ is the mean threshold potential for wave collapse [7].

During the collapse phase, the density perturbation modifies the frequencies of the localized LH states, decouples these states from the background turbulence, and quenches the energy transfer. At small scales, electric

field energy is dissipated through particle acceleration and the collapse is arrested. After the collapse is arrested ("burnout"), the cavity relaxes back to larger scales through diffusion where the nucleation process resumes.

Since collapse proceeds rapidly, Robinson [7] concluded that direct observation of this phase was improbable. Instead, nucleation and relaxation are observed where $\delta n \not\propto \mathrm{Im}(\tilde{E}_x \tilde{E}_y^*)$; this potentially reconciles the discrepancy between collapse theory [4] and Freja density and electric field observations [8,10]. In contrast to theories which focus on the collapse of a single, isolated, coherent wave packet [4], the nucleation cycle predicts the statistical properties of strong turbulence as a whole (the incoherent and coherent contributions). Under steady-state conditions, balance exists between energy transfer from the background turbulence to the nucleating states and energy dissipated through particle acceleration at arrest. The characteristic nucleation scale can be estimated from $\langle \ell_\perp \rangle \sim \langle \Phi_c \rangle / \sqrt{\langle E^2 \rangle}$ and the mean collapse threshold determined by (2) is $\langle E_c \rangle \sim \sqrt{\langle E^2 \rangle}$ where $\langle E^2 \rangle$ is the measured mean-squared electric field [5,7]. The above turbulence model implies that three-dimensional LH collapse *always* occurs at sufficiently large scale lengths under the electrostatic approximation $\langle \ell_\perp \rangle \ll c/\omega_e$.

Under the nucleation hypothesis, the field statistics of strong LHT can be divided into an incoherent contribution due to the background turbulence and a coherent contribution due to collapsing wave packets with the break point occurring at $E \sim \langle E_c \rangle$. The statistics of electric fields below threshold are described by the probability density of d-independent normally distributed isotropic random variables

$$P_d(E) = \frac{2^{1-d/2}}{\Gamma(d/2)} \left(\frac{d}{E^2}\right)^{d/2} E^{d-1} \exp\left(\frac{-dE^2}{2E^2}\right), \quad (3)$$

where d is the number of electric field components with one degree of freedom (DOF) per component. In (3) E is the instantaneous real electric field, not the complex slow amplitude which usually exhibits 2 DOF per component. The statistics of electric fields in the inertial range (above the average value of background turbulence but below the value for arrest) follow a power law scaling $P(E) \propto E^{-(d+3)}$ [5]; *this is the contribution due to self-similar collapsing structures.* Below we demonstrate that the amplitude probability distribution of the auroral LHT electric field (0–20 kHz) is accurately described by a Rayleigh distribution without the inertial power law contribution corresponding to self-similar wave collapse.

Few satellites and even fewer sounding rockets make the three-axis electric field measurements necessary to directly estimate the total electric field. However, the amplitude probability distribution of the projected electric field can be reliably estimated and compared against the theory. For example, the TOPAZ III sounding rocket, equipped with crossed Weitzmann boom assemblies deployed in the spin plane of the space craft is diagrammed in Fig. 1 [3]. The electric fields (0–20 kHz) are estimated from the potential differences between spheres mounted at the opposite ends of the $e_{x'}$ or $e_{y'}$ assemblies. The nominal baseline (distance between spheres) for the electric field measurements was 8.1 m. The spin axis of the payload was nominally oriented at an angle $\theta' \sim 90°$ relative to the $\hat{z}$ axis in a fixed coordinate system aligned with the direction of the local geomagnetic field. The electric field magnitude $\mathcal{E}$ measured by the $e_{x'}$ and $e_{y'}$ booms is related to true electric field magnitude E through the orientation (θ, ϕ) of $\mathbf{E}$ in the xyz-coordinate system and the angle θ' between the payload spin axis and z axis.

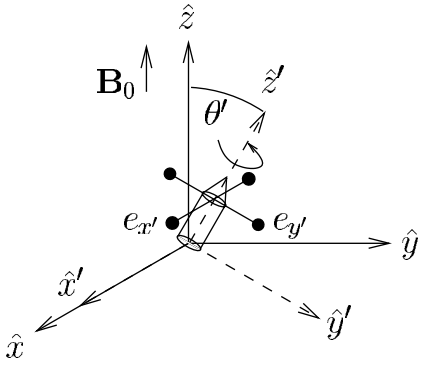

FIG. 1. Schematic diagram of a sounding rocket electric field experiment.

The theoretical amplitude probability density of the projected electric field for random turbulence is

$$\mathcal{P}_d(\mathcal{E}, \theta') = \int_0^{2\pi} d\phi \int_0^{\pi} d\theta P_d(\mathcal{E}, \theta', \theta, \phi) P(\theta, \phi), \quad (4a)$$

where

$$P_d(\mathcal{E}, \theta', \theta, \phi) = \frac{2^{1-d/2}}{\Gamma(d/2)} \left(\frac{d}{\langle E^2 \rangle \eta}\right)^{d/2} \mathcal{E}^{d-1} \left(\frac{-d\mathcal{E}^2}{2\langle E^2 \rangle \eta}\right), \quad (4b)$$

$$\eta = \cos^2\phi \sin^2\theta + (\cos\theta' \sin\phi \sin\theta - \cos\theta \sin\theta')^2, \quad (4c)$$

and $P(\theta, \phi)$ is the angular probability density of the electric field. Since LHT is nearly perpendicularly polarized ($E_z/E_\perp \lesssim \sqrt{m_e/m_i} \sim 0.006$) and randomly oriented (isotropic) in the xy plane, then the angular probability density for the electric field is

$$P(\theta, \phi) \approx \delta(\theta - \pi/2)/(2\pi). \quad (5)$$

Corrections for three-dimensional propagation and anisotropy in the plane normal to the magnetic field should be small for LHT in the oxygen-dominated auroral ionosphere.

For random LHT exhibiting d-DOF, the probability of measuring an electric field $\mathcal{E}$, when the true electric field is randomly oriented in the xy plane and the spin axis is oriented at an angle θ', is

$$\mathcal{P}_d(\mathcal{E}, \theta') = \lim_{\alpha \to 1} \frac{\mathcal{E} d \sec(\theta')}{\langle E^2 \rangle \Gamma(d/2)} \left(-\frac{\partial}{\partial \alpha} \right)^{d/2-1} \mathrm{I}_0 \left[\frac{\alpha \mathcal{E}^2 d \tan^2(\theta')}{4\langle E^2 \rangle} \right] \exp\left\{ -\frac{\alpha \mathcal{E}^2 d[1 + \sec^2(\theta')]}{4\langle E^2 \rangle} \right\}, \quad (6)$$

where $\mathrm{I}_0(z)$ is the Bessel function of the second kind. This analytic result is practical only for even values of d. However, Eq. (4) is general and may be numerically integrated for arbitrary d.

Electric field probability distributions are constructed using measurements from the TOPAZ III sounding rocket and compared with the expected probability distribution for random turbulence in two spatial dimensions perpendicular to the geomagnetic field as described by (6). The electric field probability distributions are constructed from 100 ms of data (10 per second) over 365 s of flight time near apogee (1068 km). During this time period LHSS were observed at an average rate of one per second [3]. Fewer probability distributions per second would naturally provide better statistics. Unfortunately, the analysis is limited by interference from the mechanical vibrations at about 0.2 Hz (see discussion below). The five free parameters required to fit (6) to the experimental data consisted of the following: the amplitude of $\mathcal{P}_d(\mathcal{E}, \theta')$, the angle θ', the expected true mean-squared electric field $\langle E^2 \rangle$, and the dc offsets of the $e_{x'}$ and $e_{y'}$ electric field booms which may change in response to low-frequency turbulence $f \ll f_{\mathrm{R}}$. The data were fitted by nonlinear minimization of the chi-squared statistical parameter with $d = 2$ or 4 in (6). The mean reduced chi squares were $\langle \tilde{\chi}^2_{d=2} \rangle = 1.0 \pm 0.3$ and $\langle \tilde{\chi}^2_{d=4} \rangle = 7.6 \pm 1.6$, respectively. The LHT observed by TOPAZ III is consistent with the two-dimensional random turbulence ($d = 2$ DOF); only 0.2% of the distributions were compatible with $d = 4$. Henceforth only the properties of the $d = 2$ fit parameters will be discussed.

Figure 2 shows amplitude probability distribution of LHT detected between 465.4 and 465.5 sec after launch. The curve fit has a $\tilde{\chi}^2_{d=2} \approx \langle \tilde{\chi}^2_{d=2} \rangle = 1.0$ with 29 DOF. The probability that $\tilde{\chi}^2$ would be as large or exceed this value by chance is 48%. The fitting parameters are $\theta' = 83.8 \pm 0.9°$ and $\langle E^2 \rangle = 319 \pm 0.5\ (\mathrm{mV/m})^2$. Figure 3 shows the fit parameters from (6) with $d = 2$ during 365 s of data. The top panel is θ', the angle between the spin axis and the geomagnetic field. The solid line is the angle computed from the onboard three-axis flux-gate magnetometer. The oscillation ($f \sim 0.024$ Hz) reflects precession of the payload spin axis with respect to the magnetic field. The mild secular decay of the angle over the 350 s interval indicates energy loss from the system. The magnetometer data accurately capture the upper envelope of θ' parameters from the fitted probability distributions. However, there is a small spread in the θ' parameters away from the line computed from the magnetometer data. This spread is primarily produced by mechanical vibrations of the electric field booms (discussed below). The bottom panel of Fig. 3 is $\langle E^2 \rangle$, the expected true mean-squared electric field, and $\sqrt{\langle E^2 \rangle}$ exceeds 15 mV/m during most of this time period. According to (2) with $\Omega_{\mathrm{e}} \sim 2\omega_{\mathrm{e}}$ and $T_{\mathrm{i}} = T_{\mathrm{e}} = 0.3$ eV $= 3500$ K, the mean nucleation scale during this time period is $\langle \ell_\perp \rangle \lesssim 4$ m which is much shorter than the scale sizes observed by TOPAZ III. The top panel of Fig. 4 shows the power spectrum of θ' computed from the data in Fig. 3. Narrow-band deterministic peaks can be observed at multiples of 0.19 Hz, the largest occurring at about 0.77 Hz. The fundamental fully extended cantilever resonance of a single boom was measured at 0.76 Hz by Weitzmann Consulting, Inc., the spin frequency of the payload was 0.1 Hz, and the estimated fundamental resonance

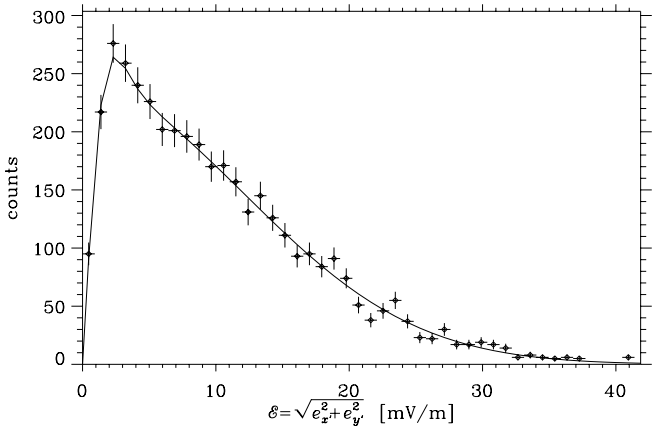

FIG. 2. Amplitude probability distribution of LHT detected between 465.4 and 465.5 sec after launch.

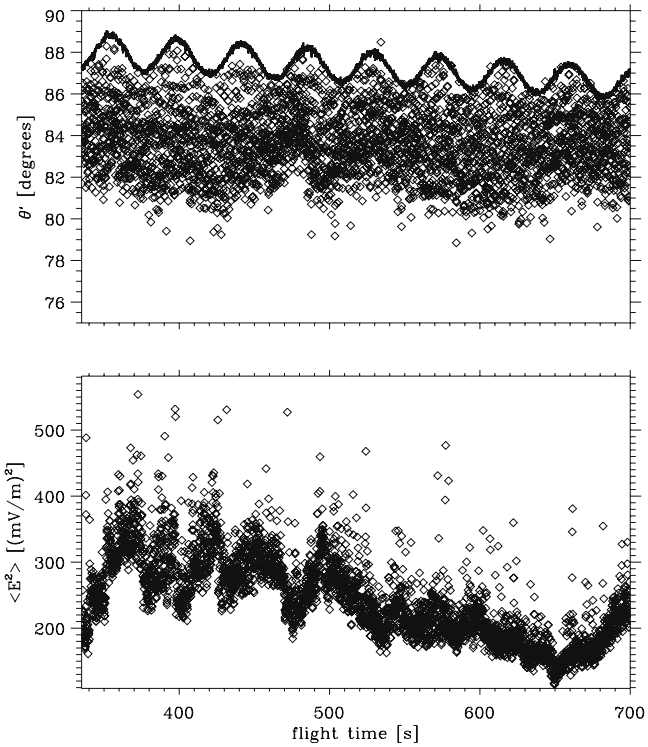

FIG. 3. Fit parameters of (6) with $d = 2$ to 365 sec of data from the TOPAZ III flight (see text).

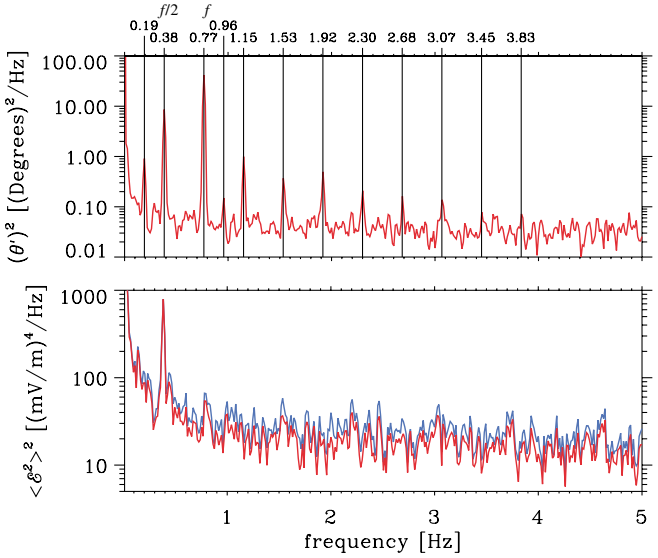

FIG. 4 (color). Top: Power spectrum of θ'. Bottom: Power spectrum of $\langle \mathcal{E}^2 \rangle$ measured (blue) and $\langle \mathcal{E}^2 \rangle$ predicted (red). The fundamental and half-harmonic frequencies of the boom vibrations are indicated by the labels f and $f/2$.

frequency of the boom-payload dynamical system is $f = \sqrt{0.76^2 + 0.1^2} \approx 0.77$ Hz. Thus, we conclude that the primary peak at 0.77 Hz is produced by resonant oscillations of the boom-payload system. The other narrow-band features in Fig. 4 could be caused by direct or parametric pumping of boom vibrational modes. The bottom panel shows the measured power spectrum of $\langle \mathcal{E}^2 \rangle$ (blue) and expected power spectrum (red) determined from the fit parameters by $\langle \mathcal{E}^2 \rangle = \langle E^2 \rangle [3 + \cos(2\theta')]/4$. The two spectrums agree quantitatively over the frequency range shown. The large anomalous peak at 0.38 Hz is caused by the boom oscillations modulating the observed and inferred electric field. The complicated nonlinear dynamics of the boom-payload dynamical system is not well understood. However, the boom vibrations can change the apparent angle of the electric field instrument with respect to the payload spin axis and shorten the effective baseline. The sensitivity of (6) to the boom vibrations implies that (3) is accurate for *all* values of electric fields observed here.

This analysis did not focus on individual LHSS for three reasons: First, the nucleation cycle hypothesis predicts the amplitude probability density of the coherent and incoherent turbulence simultaneously so there is no need to bias the statistics by considering just data segments containing LHSS. Second, LHSS electric fields frequently exhibit signatures characteristic of double layers produced by payload potential variations in the density depletion [3]. Consequently, determining the probability distribution of the electric field within an individual LHSS without first removing the double layer signature is impossible. Last, the electric fields outside LHSS show little if any discernible phase shift across the electric field interferometer [3]. Thus, the electric field instrument is most accurate in the ambient plasma.

The amplitude probability distribution of LH electric field turbulence in a region where hundreds of LHSS are observed is accurately described by the Rayleigh distribution for *weak* turbulence where E_x and E_y are statistically independent Gaussian random processes. The mean decoherence time [12] of the spectrum is $\langle \tau_d \rangle = 31 \pm 6$ μs, much shorter than a lower-hybrid period $\tau \sim 1/f_R \sim 200$ μs which implies that auroral LHT can be accurately described by a random process [13]. Neither the amplitude probability distribution nor the power spectrum exhibits any evidence of the coherent process necessary to drive the global modulational instability.

These data do not exhibit the power law inertial range, the statistical characteristic of self-similar collapse, predicted by Robinson [5,7]. Generally, LH collapse [4,5,7] is not realized, occurs too quickly, or initiates at scales too close to the arrest scale for self-similar statistics to develop. However, these results *are* consistent with nucleation and resonant scattering in preexisting density depletions. Direct nucleation of energy into bound states occurs if the background density varies adiabatically with respect to the LH frequency [11]. Previous observations suggest that resonant scattering is observed far more frequently than nucleation [9]. The nucleation and scattering mechanisms should not significantly affect the global statistical properties of the amplitude probability distribution for LHT because neither process is amplitude dependent. While the modulational instability and collapse cannot be rigorously ruled out by experiment, we conclude that this paradigm [4,5,7] is *irrelevant* to statistical properties of at least the great majority of LHT data collected in the auroral ionosphere at sounding rocket altitudes.

We acknowledge useful conversations with John Bonnell, Ira Schwartz, Bahman Hafizi, Steve Powell, and Julie Schuck. This work was supported by ONR.

*Electronic address: schuck@ppdmail.nrl.navy.mil

[1] V. E. Zakharov, Zh. Eksp. Teor. Fiz. **62**, 1745 (1972) [Sov. Phys. JETP **35**, 908 (1972)].
[2] P. M. Kintner *et al.*, Phys. Rev. Lett. **68**, 2448 (1992).
[3] J. L. Vago *et al.*, J. Geophys. Res. **97**, 16 935 (1992).
[4] V. D. Shapiro *et al.*, Phys. Fluids B **5**, 3148 (1993).
[5] P. A. Robinson, Phys. Plasmas **3**, 192 (1996).
[6] V. D. Shapiro, Phys. Rev. Lett. **81**, 3415 (1998).
[7] P. A. Robinson, Adv. Space Res. **23**, 1679 (1999).
[8] H. L. Pécseli *et al.*, J. Geophys. Res. **101**, 5299 (1996).
[9] J. W. Bonnell *et al.*, Phys. Rev. Lett. **80**, 5734 (1998).
[10] S. H. Høymork *et al.*, J. Geophys. Res. **105**, 18 519 (2000).
[11] G. D. Doolen *et al.*, Phys. Rev. Lett. **54**, 804 (1985).
[12] The decoherence time is determined from the first zero of the autocorrelation function.
[13] This implies that the expectation value of the ponderomotive potential in (1) is zero.